AD-A193 898 REFLECTION AND SCATTERING OF ACOUSTIC RAYS COMPUTED FOR PARABOLIC ICE KEEL MODELS(U) NAVAL OCEAN SYSTEMS CENTER SAN DIEGO CA D F GORDON APR 88 NOSC/TR-1217 1/1

UNCLASSIFIED F/G 20/1 NL

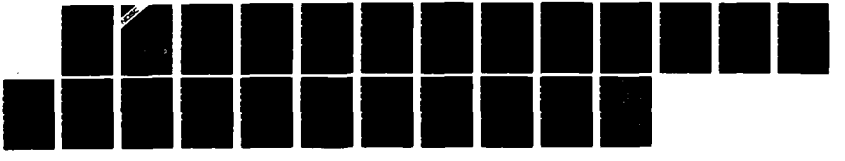

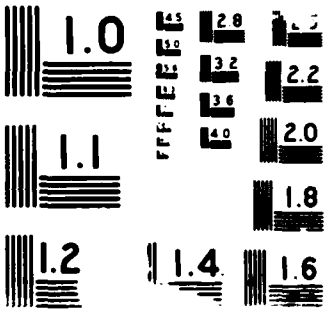
1.0
1.1
1.2
1.4
1.6
1.8
2.0
2.2
2.8
3.2
3.6
4.0

(4)

NOSC TR 1217

NAVAL OCEAN SYSTEMS CENTER San Diego, California 92152-5000

Technical Report 1217
April 1988

Reflection and Scattering of Acoustic Rays Computed for Parabolic Ice Keel Models

D. F. Gordon

NAVAL OCEAN SYSTEMS CENTER

San Diego, California 92152-5000

E. G. SCHWEIZER, CAPT, USN
Commander

R. M. HILLYER
Technical Director

ADMINISTRATIVE INFORMATION

This report describes work done under NOSC Independent Research (IR) funds for fiscal year 1987. The work utilizes computer programs developed under IR funding in fiscal years 1984 and 1985 for the acoustic analysis of single ice keels.

Released by
E.F. Rynne, Head
Acoustic Analysis Branch

Under authority of
T.F. Ball, Head
Acoustic Systems and
Technology Division

8a. NAME OF FUNDING/SPONSORING ORGANIZATION	8b. OFFICE SYMBOL (if applicable)	9. PROCUREMENT INSTRUMENT IDENTIFICATION NUMBER
NOSC Independent Research	Code 013	

8c. ADDRESS (City, State and ZIP Code)	10. SOURCE OF FUNDING NUMBERS			
	PROGRAM ELEMENT NO.	PROJECT NO.	TASK NO.	AGENCY ACCESSION NO.
San Diego, CA 92152-5000	61152N	RR00001		711-ZT69

11. TITLE (include Security Classification)

REFLECTION AND SCATTERING OF ACOUSTIC RAYS COMPUTED FOR PARABOLIC ICE KEEL MODELS

12. PERSONAL AUTHOR(S)

D.F. Gordon

13a. TYPE OF REPORT	13b. TIME COVERED	14. DATE OF REPORT (Year, Month, Day)	15. PAGE COUNT
Research Report	FROM Oct 1986 TO Oct 1987	April 1988	24

16. SUPPLEMENTARY NOTATION

17. COSATI CODES			18. SUBJECT TERMS (Continue on reverse if necessary and identify by block number)
FIELD	GROUP	SUB-GROUP	Arctic acoustics; Acoustic propagation; Ray theory; Sea ice; Reflection coefficients; Scattering coefficients; Ice keels

19. ABSTRACT (Continue on reverse if necessary and identify by block number)

Coefficients are computed for ray reflection and scattering from a model of a set of keels. The model is a collection of parallel ice keels that are of parabolic cross section. The size of the keels and the spacing between them are drawn from random distributions. The keels are also widened by a random factor to simulate oblique incidence on nonparallel keels. Rays are permitted to reflect from and refract through keels according to the interface properties between fluids and elastic solids. A large number of rays are directed toward the keel model and, upon emergence, are sorted into angular bins to determine scattering strength versus direction. Scattering coefficients have a dominant lobe near the secular direction. This is shown to result from the shape of the curve of reflection versus grazing angle. Very little backscatter occurs, a result of the limited slope angle of the parabolic keel models.

20. DISTRIBUTION/AVAILABILITY OF ABSTRACT	21. ABSTRACT SECURITY CLASSIFICATION
☐ UNCLASSIFIED/UNLIMITED ☒ SAME AS RPT ☐ DTIC USERS	UNCLASSIFIED

22a. NAME OF RESPONSIBLE INDIVIDUAL	22b. TELEPHONE (include Area Code)	22c. OFFICE SYMBOL
D.F. Gordon	(619) 553-1455	Code 711

SUMMARY

OBJECTIVE

Determine the high-frequency acoustic scattering characteristics of a random set of ice keels.

APPROACH

Parabolic sections were used to represent ice keels that are random in size and spacing. A large number of rays were computed to model the interaction of a plane wave with the random set.

RESULTS

The principal results of this work are diagrams of scattering strength versus angle as functions of incident angle. Reflection loss data in the specular direction are also given.

CONCLUSIONS

1. Plane wave reflection coefficients strongly control the scattering action of the set of keels.
2. At grazing angles below 20 degrees, transmission through the keels as shear waves is the dominant energy path.
3. Specular reflection is determined predominantly by the extent of unshadowed surface.
4. The parabolic-shaped keels underestimate backscatter from the keels.

RECOMMENDATIONS

1. Determine and paramaterize the shapes and internal structure of real keels, and if substantial variation is observed, determine probability distributions for these parameters.
2. Use compound figures to model realistic keel shapes and their acoustic properties.
3. Include internal structure and attenuation in models
4. Seek experimental verification for acoustic results reported here.

CONTENTS

INTRODUCTION

The scattering of rays by a random collection of ice keels has been investigated by the Naval Ocean Systems Center (NOSC). This report presents the results of this investigation. The computer ray program used in this project was reported at the Austin meeting of the Acoustic Society of America in April 1985 and in Ref. 1.

In a 1976 article in the Journal of the Acoustic Society of America (Ref. 2), O.I. Diachok showed that Twersky's boss-scattering theory was an effective approach to underice scattering and propagation. A first-term approximation from that theory was shown to give effective results for high frequencies, as did another at low frequencies. The current task derives high-frequency numerical values similar to the former, the main difference being that the individual bosses are of random size.

This report will first discuss the random ice keel model used, and then the ray computation technique. There will then be a discussion of two functions that were derived or estimated, the angular distribution of rays scattered from the set of keels and the specular scattering coefficient. The final section will discuss some of the geometry and mechanics of the computations to explain various observed features of the computed functions. These discussions will aid in determining which results arise from given assumptions of the model and provide a basis for estimating the acoustic properties of real keels. Such estimations, however, are not attempted here. An alternative view of ice keels, in which their rough or block character is emphasized, has been provided by S. Chin-Bing (Ref. 3).

COMPUTER METHOD

Figure 1 indicates the basic computational strategy. A large number of equally spaced rays are launched towards a set of keels represented as parabolas. As the rays emerge from the set of keels, they are accumulated in angular bins. The contents of these bins then represent the scattering characteristics of the keel set. The distance between keels is random, drawn from a rectangular distribution to give 9.5 keels/ km. The depths of the keels are drawn from a Rayleigh distribution with a mean depth of 4 m. A further parameter, the ratio of depth to width is 1 to 3.2. Therefore, the keels are all similar geometric figures. Most of these parameters are taken from Diachok's 1976 article.

Figure 2 shows details of an individual keel on an equal length-depth scale. This is the cross section of an elongated object. For simplicity the keel is assumed to be infinite in length. The maximum slope of the keel edge is at its upper edge and is 51.3 degrees. The keel model as shown was next modified to simulate an orientation of the keels that is random when viewed from above. This was done by increasing the width of the keels by a function of a random angle between 0 and 90 degrees — approximately the secant of the angle. However, this function is modified by the fact that, in a given range interval, one is more likely to cross a keel perpendicular to a path than one nearly parallel.

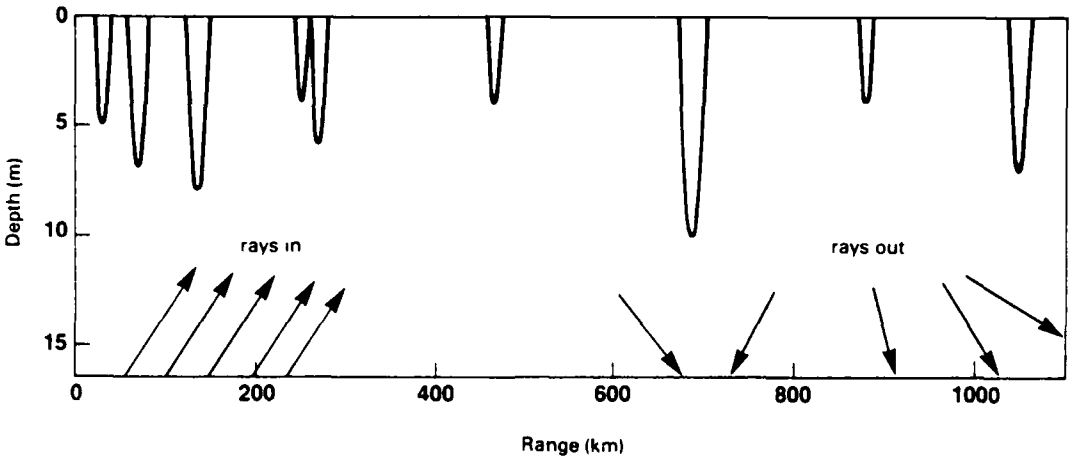

Figure 1. Model of a random set of ice keels, with incoming and scattered rays suggested by the arrows.

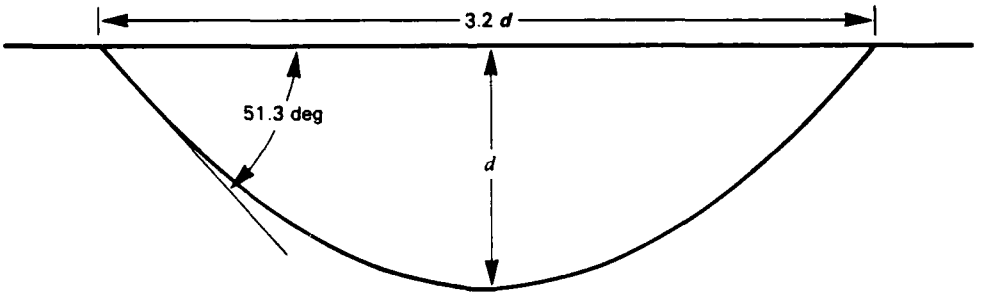

For random orientation:
Multiply width by $(1 - x^2)^{-1/2}$
where x is random, $0 < x < 1$

Figure 2. Cross section of a keel model. The equation gives the widening factor caused by oblique incidence on a randomly oriented keel.

If our line of sight is crossed by a keel of width w at an angle of incidence of θ, then the apparent width of the keel is sec θ. The probability of crossing a randomly oriented keel at angle θ must be derived.

This probability is proportional to cos θ. By symmetry, θ can be confined to the interval from 0 to 90 degrees. The probability distribution function is therefore cos θ, $0<\theta<90$ degrees and zero elsewhere. The cumulative distribution function of θ is therefore sin θ over the same interval. A random value of θ from this distribution can now be picked by taking arcsin (x) where x is uniformly random from 0 to 1. The desired width of this randomly selected keel, W, is then w sec [arcsin(x)] or

$$W = w(1 - x^2)^{-1/2} \tag{1}$$

This formula is repeated on Fig. 2.

Figure 3 shows three sample keel sets that were used to estimate scattering. They will be identified in the remainder of this report as sets A, B, and C. Sigma indicated on each one is the standard deviation of ice depth in meters. As can be seen, there is considerable variation in this parameter, although the three sets were generated by selecting random values from the same distributions. If the three sets are combined into one long set, it has a sigma of 2.1 m, or nearly average for observed Arctic ice roughness.

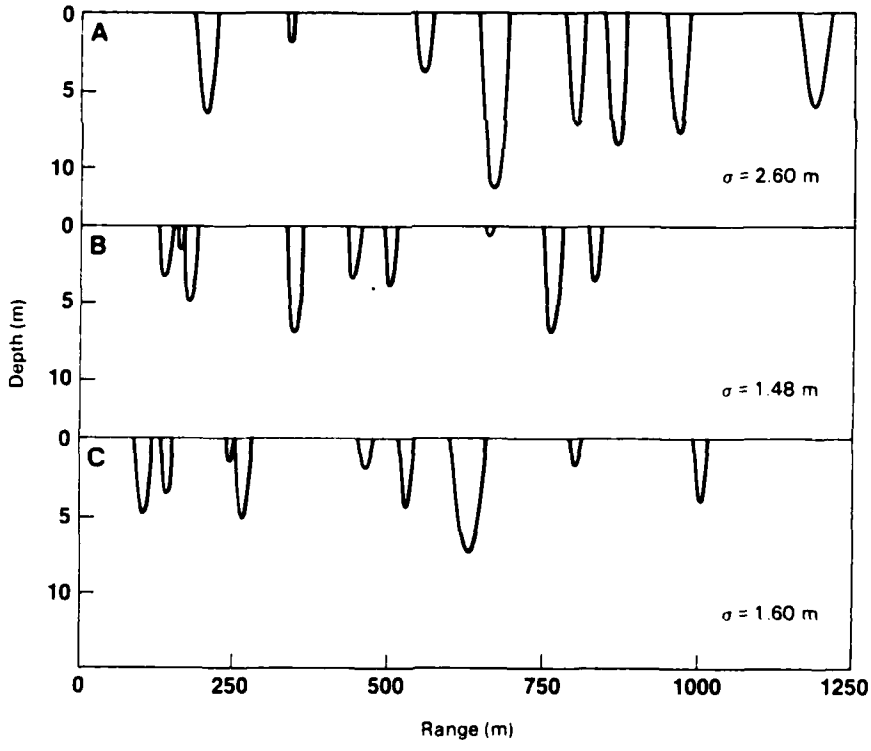

Figure 3. Three keel sets generated by random numbers. The standard deviation of ice depth is given on each set.

Ray scattering functions were derived as follows. A number of rays were launched at the same angle, but at successive ranges to simulate a plane wave directed at the keel set at a given angle of incidence. Usually 800 rays were used. Rays leaving the keel set and crossing a given receiver depth are sorted into angular bins. Any reflection of transmission losses at boundaries alters the intensities of the accumulated rays. Spreading loss is accounted for by the collection into angular bins. Rays are equally spaced along the plane wave front and therefore represent equal energy. The sum of ray contributions in any bin is a measure of relative intensity.

Two scattering processes are allowed in the computations: reflection at the ice-water interface and refraction through the keel. Refraction is permitted at both the shear and compressional speed in the ice. However, few rays strike the keels at sufficiently large grazing angles for transmission at the compressional speed, so shear wave paths through the keels predominate. Edge-diffracted rays were included in Ref. 1. But since their contribution to the field is small, they are not included here.

The computer program used here requires a non-zero sound speed gradient, so the rays will have curvature. Since our purpose here is to determine the scattering properties of the set of keels, we prefer straight line rays. The curvature is minimized by using a small gradient and by placing source and receiver depths just below the keels. These depths were usually 10 or 20 m, depending on the deepest keels in the set. A sound-speed gradient of 0.0002 sec^{-1} was used in all computations here.

The reflection and transmission properties of ice can be computed following Ewing, Jardetsky, and Press (Ref. 4). The acoustic parameters required are the sound speed in the water, the shear and compressional sound speeds in the ice, and the density of water and ice. Table 1 shows the values of these parameters used here. These are typical observed values for Arctic sea ice. The shear speed varies over a large range of values, depending on the condition of the ice. Observed values easily vary from 1400 to 2200 m/s.

Table 1. Typical acoustic parameters in Arctic sea ice and water.

Parameter	Value
Sound speed in water	1440 m/s
Compressional sound speed in ice	3600 m/s
Shear sound speed in ice	1600 m/s
Water density	1026 kg/m^3
Ice density	920 kg/m^3

SCATTERING RESULTS

Figure 4 shows the angular distribution of scattered rays. The sum of rays in each 2-degree angular bin is expressed as a decibel by taking -10 log of the ratio of the ray sum in a bin to the total rays launched. Keel distribution A of Fig. 3 was used. The surprising result here is that almost all rays are scattered into the forward direction. Very small backscattering lobes can be seen for the steeper rays. Note also that a significant specular component does not show up for angles of incidence below 6 degrees.

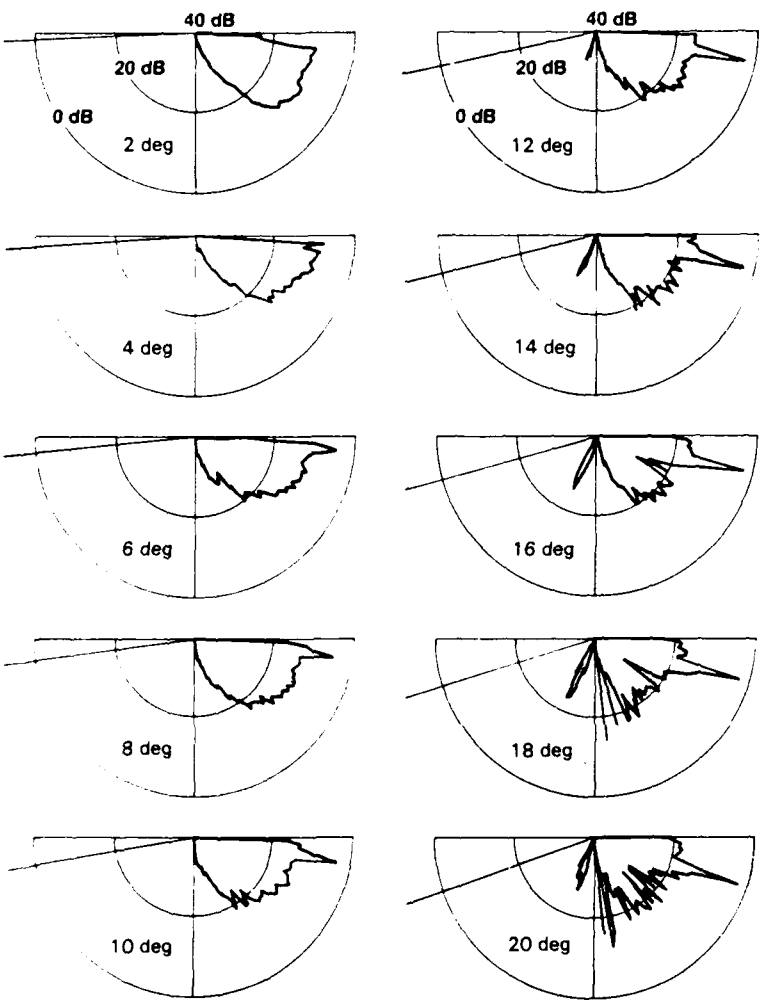

Figure 4. Energy scattered into 2-degree bins as a fraction of total energy in a plane wave striking keel set A at the designated angle (grazing angle for a ray).

The small backscatter is an unrealistic result because of the limited slope angles of the parabolic keels. This will be discussed in later sections, which give detailed analyses of the mechanics creating these curves. In general, the predominance of forward scatter over backscatter results from the water-ice reflection coefficients. One set of plane wave reflection and transmission coefficients is shown in Fig. 5. There are similar sets of reflection coefficients for the shear and compressional waves impinging on the ice-water interface. The sea ice shear sound speed of 1600 m s from Table 1 gives a critical grazing angle of 26 degrees. Below this angle, perfect reflection occurs for lossless media. Above this angle, the reflection loss increases rapidly. Simultaneously the transmission loss into shear waves decreases rapidly. The ice becomes very transparent to the sound. This transparency at high grazing angles is a major cause of the preferential forward scatter of the rays.

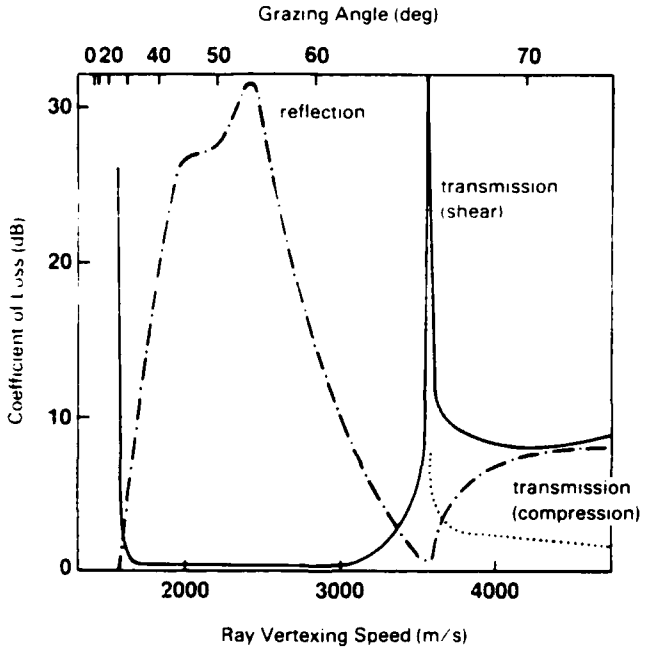

Figure 5. Plane wave reflection and transmission coefficients at a water-ice interface for a compressional wave in the water.

Figure 6 shows angular scattering diagrams for three angles for the three keel sets of Fig. 3. Set A has a considerably higher roughness factor, or sigma, than sets B or C. However, no distinctly different characteristics are apparent in set A.

Figure 7 gives an idea of what part of the scattered energy is contributed by reflection and what part by refraction through the keels. Figure 7 is equivalent to panel A in Fig. 6, but only the reflected rays are included. As can be seen, the refracted energy accounts for a predominant part of the scattered field. This refracted energy tends to remain closer to the specular direction, with the reflected energy accounting for much of the higher angle scatter.

The specular reflection coefficient is the product of this investigation that is most immediately usable in propagation loss programs. It essentially measures the energy that remains coherent upon reflection from the rough surface. Figure 8 shows this reflection coefficient as a function of grazing angle for the three keel sets. Below a grazing angle of 6 degrees, the larger roughness of set A seems to produce a larger scattering loss. At larger

angles, the roughness seems immaterial. The rays that contribute to this specular reflection are almost all those that reflect from the smooth surface without touching a keel. The function shown here is thus a measure of the unshadowed surface as seen from both the source and receiver.

Theory for constant-depth bosses holds that the reflection loss, which becomes large at low grazing angles, should recover at very low angles and become zero at zero-degree grazing angles. However, computations with this program down to 0.75 degree have shown no tendency towards recovery of the reflection loss.

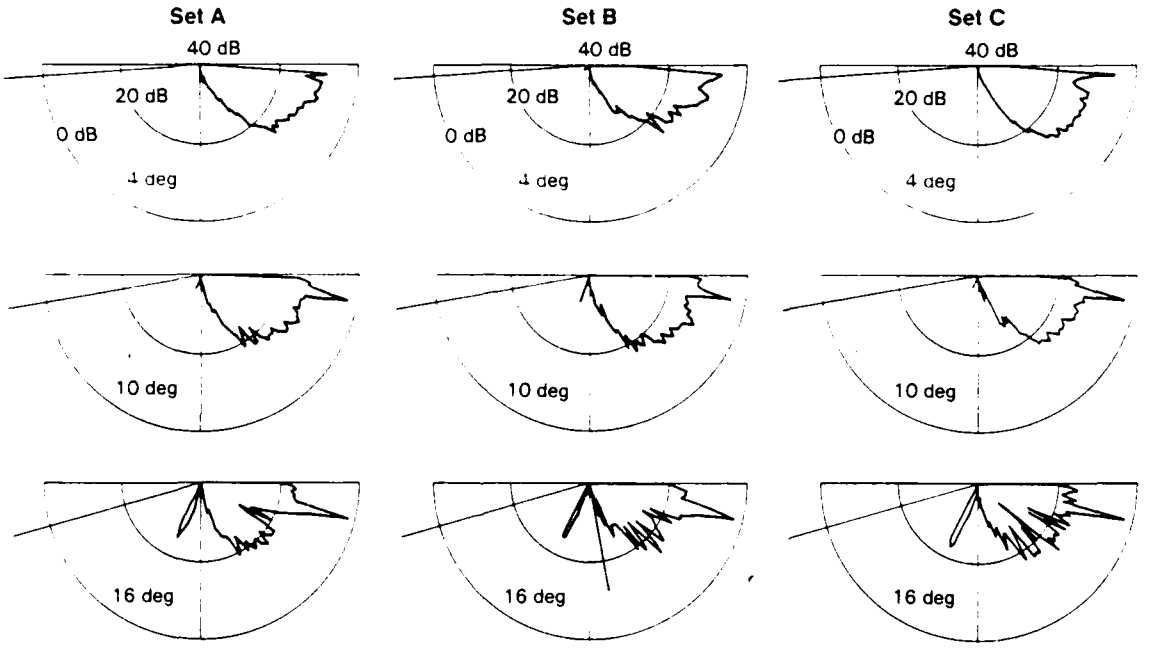

Figure 6. Angular scattering functions by 2-degree bins for keel sets A, B, and C.

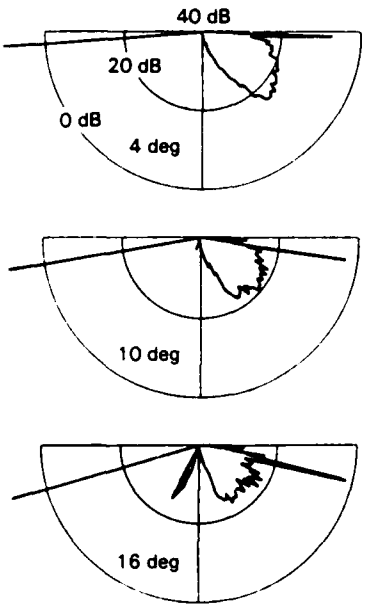

Figure 7. Angular scattering function for keel set A, where only reflected rays are used. Transmitted rays are omitted.

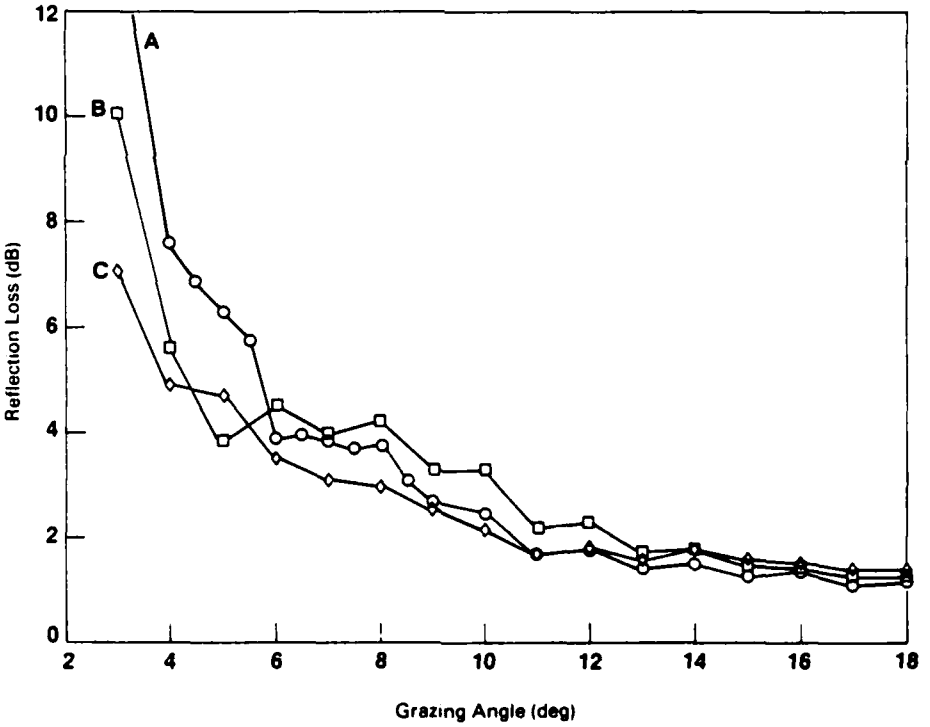

Figure 8. Specular scattering coefficients as a function of grazing angle for the three keel sets. These are equivalent to the scattering function values in the 2-degree bin containing the specular angle.

GEOMETRIC IMPLICATIONS OF SCATTERING ANGLES

In this section the general shape of the scattering functions will be discussed. In particular, the backscattering function will be shown to be underestimated because of the limited slopes of the ice model. This topic is discussed first because it is important that the backscatter functions of this report not be used for estimation or modeling purposes. A geometric discussion of the specular reflection function and the scattering curves will follow to explain some of the features of these curves.

BACKSCATTER

Two notable features of such scattering curves as those of Fig. 4 and 6 are the null in the downward direction and the small backscattering lobes. Both these features result from an interplay between the parabolic shape and the reflection coefficient. Figure 5 shows reflection and transmission losses for a water-ice interface. These are computed by the method of Ewing, Jardetsky, and Press (Ref. 4). Table 1 gives the acoustic parameters used. Computations of the reflection loss for a wide range of these parameters are given by Mayer, Behravesh, and Plona (Ref. 5). Although the losses in Fig. 5 are plotted as functions of the phase velocity, an equivalent grazing angle scale is given at the top of the figure.

As a result of the acoustic parameters chosen here, acoustic energy begins to penetrate the ice-water interface at a grazing angle of about 26 degrees. The next increase in grazing angle of a few degrees finds almost all energy transmitted into the ice via the shear wave and almost none reflecting. At an angle of 45 degrees, less than 1% of the energy is reflected. A ray reflecting from a sloping surface is diverted by twice the slope of the surface. (Exact expressions will be given later.) The rays scattered downward near 90 degrees have reflected from a slope near 45 degrees and hence suffered a large reflection loss. The nulls in the downward direction on the scattering curves are images of the null in the reflection coefficient of Fig. 5.

Near a grazing angle of 66 degrees the compressional wave in the ice is excited. From this angle on to 90 degrees 10% or more of the energy is reflected. Figure 5 shows good reflection coefficients starting at about 60 degrees. Such slopes will reflect at 120 to 180 degrees or backscatter the energy. However, the parabolic ice keels used in this study have maximum slopes of 51.3 degrees. Therefore only a few of the rays of highest incident angles can reach these good reflectors for backscatter.

To test the assumption that higher slope angles would produce more backscatter, a run was made with keels of half width. This was a relatively simple test to make. The keels of set A were reduced to half their width, with all other parameters remaining the same. This increases the maximum slope angle from 51.3 to 68.2 degrees. This should permit many more rays to fall into the preferred grazing-angle range. The additional 17 degrees should increase the backscattered angular bins to angles about 34 degrees higher. Figure 9 shows the results, leaving little doubt that the higher slope angles do control the backscatter and that if all slopes up to 90 degrees occurred in the model, the backscattered field would be continued completely around to 180 degrees. The accuracy of such a field would depend on the overall accuracy of the ice keel model.

Figure 9 shows that slopes above 51.3 degrees increase the backscattered field. However, the forward-scattered fields should not be accepted in the place of those of Fig. 6 because the modeled keels do not have dimensions equal to the best estimates of real ice keels.

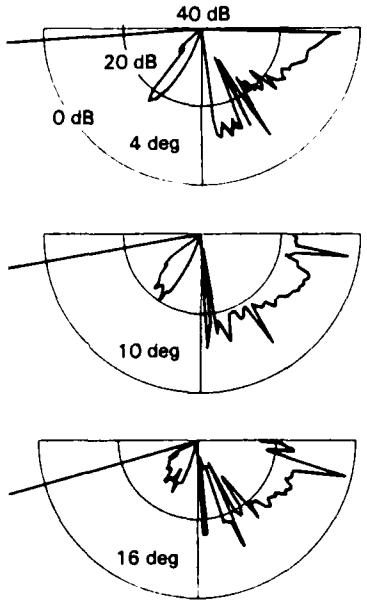

Figure 9. Angular scattering functions for a set similar to keel set A, except that the keel width is reduced by half.

SURFACE SHADOWING

The curves of Fig. 8 appear to be a measure of the unshadowed surface. In the following discussion, a theoretical derivation of the shadowing under simplifying assumptions will be derived and compared with the model results. Let us remove the randomness and assume that the keels are evenly distributed, 9.5/km, and have a depth of 4 m. These are the means of the uniform and Rayleigh distributions from which the random sets were made. We need to compute for plane wave angle θ the fraction of surface not shadowed by the keels, f, and convert to decibels by taking $-10 \log f$. A general expression will be given first. Figure 10 shows the wave front, s, for a ray angle of 30 degrees for a specific keel. Rays that reflect in front of and then strike the keel are represented by use of a reflection of the keel on the surface.

Let d be the depth, b the half width of the keel, and s_i the length along the approaching plane wave front that will intersect the keel. Then

$$s_i = [\ (b^2 \tan^2 \theta + 4bd \tan \theta + 4d^2) \cos \theta]/4d \qquad (2)$$

The width of wave front that intersects the keel after reflection in front of the keel is given by changing the sign of θ.

Thus the total length of wave front intercepted, s_t, is

$$s_t = [\ (b^2 \tan^2 \theta + 4d^2)\cos \theta]\ /\ 2d \qquad (3)$$

The surface length shadowed by this length of wave front is $s_t / \sin \theta$. These equations apply up to the maximum slope angle of the keel, ϕ_{max}, or

$$\phi_{max} = \arctan(2d/b) \qquad (4)$$

At greater values of θ, the shadow is just the width of the keel.

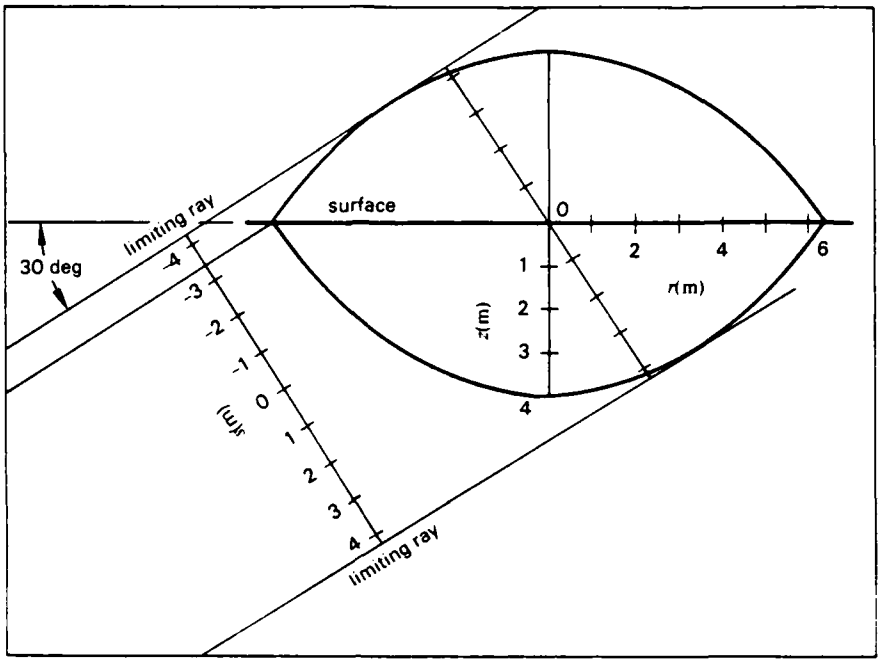

Figure 10. Portion of a plane wave front intersecting a keel and its reflection on the surface. A coordinate axis labeled s is centered on this wave front.

The half width b was 1.6 d in the original distribution. This gives a maximum slope angle of 51.34 degrees. Since the keels were randomly widened by Eq. 1 to simulate random directional orientation of the keels, a larger value of b is appropriate. The mean widening factor can be determined by integrating Eq. 1 from 0 to 1. A value of $\pi/2$ is obtained. This gives an average half width of 10.05 m, compared with 6.40 m without widening. The percent of shadow for b = 10.05 m and converted to decibels as described above is plotted in Fig. 11. The ray theory values from Fig. 8 are included for comparison. The shadow covers the complete surface at a grazing angle of 4.39 degrees, and the loss is infinite. At almost all angles above 8 degrees this surface shadow curve lies within the ray theory data points. The smaller loss of the ray theory over the shadowing curve for angles below 7 degrees may result partly from scattered rays falling into the 2-degree bins in which rays are collected. However, the largest difference arises from the randomness of the keels, which do not shadow the surface as efficiently as do keels of uniform size and spacing.

A quick correction for this effect is to assume that the shadows are randomly spaced and subtract the fraction of double-shadowing from the fraction of shadowed surface, giving x^2 2, where x is the probability of a point on the surface being shadowed. This shadowed fraction is in turn corrected for triple shadowing, and so on. This series is a representation for the exponential function, a familiar result from probability theory. Thus the unshadowed surface $1-x$ is represented by $\exp(-x)$. The lower line in Fig. 11 shows this loss for a randomly shadowed surface. The resulting curve seems to serve as a lower limit to the reflection loss.

Had we used the narrower keels having a half width of 6.4 m, the upper line would have been very similar. It is about 0.22 dB less at 5 degrees, 0.10 dB less at 10 degrees, and back up to 0.15 dB less at 20 degrees. These narrower keels fully shadow the surface at a 4.37-degree grazing angle. The shadowing strength of the keels depends very little on their width, but rather on depth and spacing.

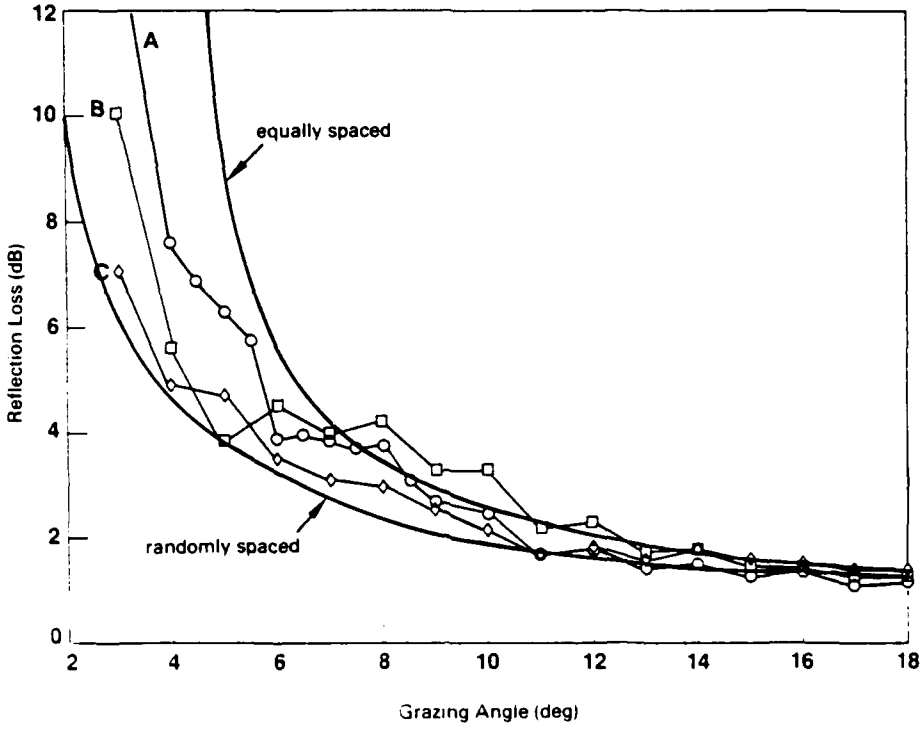

Figure 11. Estimated specular reflection coefficients are compared with those determined by accumulating rays. The upper estimate is based on evenly spaced, similar keels. The bottom estimate is based on randomly spaced, similar keels.

SCATTERING FUNCTIONS

The scattering functions are a sum of the reflected and refracted fields. A full analytical description of neither of these fields is attempted in the following discussion. However, some equations and plots are given to clarify some aspect of the fields.

Returning to Fig. 10, the slope of the parabola at the point a ray strikes can be determined. The ray is defined by the value of s or distance from the center of the wavefront that intersects the keel. The angle of the wave front, θ, is defined as the angle the rays make to the horizontal, where the angles of rays arriving from below the horizontal are positive. The slope of the parabola ϕ is given by

$$\phi = \tan^{-1}[\, -2dr \cdot (b^2)] \tag{5}$$

where the intercept range, r, is given by

$$r = \{ (\tan\theta) \cdot (d/b^2) - [\, (\tan^2\theta)/(d^2/b^4) + 4(d - s/\cos\theta)/(d/b^2)^{1/2}\}/2$$

Figure 12 summarizes the use of these last two equations for the keel of Fig. 10. It is a plot of certain slope values at points of intersection between a ray and the keel. The rays are determined by ray angle θ and s, the position on the wave front as defined in Fig. 10. The two lines labeled "limiting ray" are the tangent rays, and they intersect the parabola where its slope is $-\theta$. The angle between ray and parabola is $\theta + \phi$ or zero at the point of tangency. The width

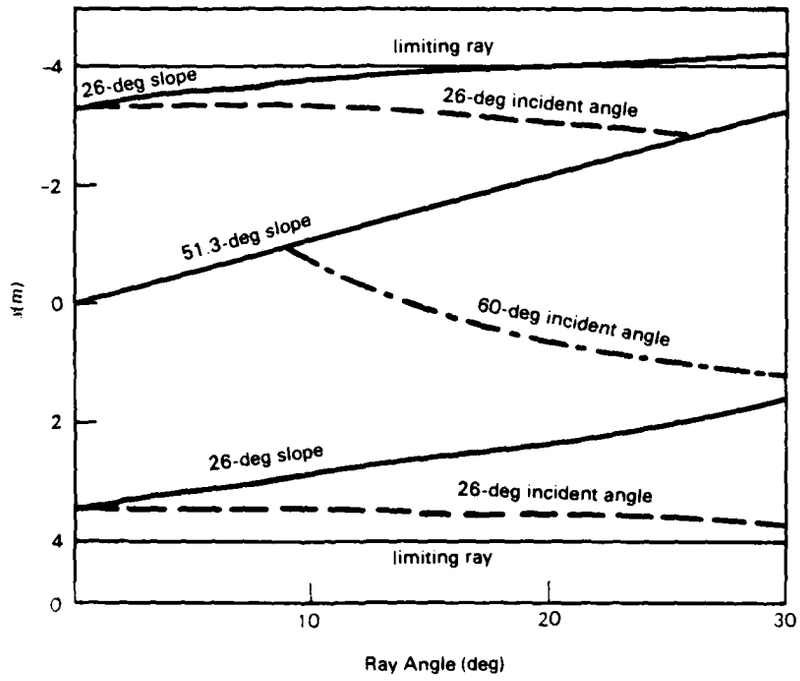

Figure 12. Locus of points along the wave front from which rays of a given grazing angle strike the keel at designated angles.

between these limiting rays increases by only 0.4 m from a ray angle of 0 to 30 degrees. The maximum slope of 51.3 degrees occurs where the keel meets the surface, so the ray reaching this point is the boundary between the direct rays and the surface reflected rays. As can be seen from the 51.3-degree line in Fig. 12, as the grazing angle increases, a growing proportion of the wave front intersects the keel directly and a decreasing portion intersects the keel after reflection from the surface. The proportion would reach zero if the figure were extended to a ray angle of 51.3 degrees.

The slope of 26 degrees is of interest because, as was discussed earlier, at grazing angles of 26 to 60 degrees the rays are largely transmitted into the ice. The locations of rays that intersect the keel where its slope, or ϕ, is 26 degrees are labeled 26-degree slopes on the figure. However, of more interest are the rays for which $\theta + \phi$ is 26 degrees. This is the true dividing line between reflected and transmitted rays. Rays with this property are shown by dashed lines in the figure. Note that only about 15% of the rays are perfectly reflected. Most of the rest meet the keel at angles that favor transmission through the keel as a shear wave. However, at an incident angle above 60 degrees there is a more even split between reflected and transmitted rays. The wedge between the lines labeled "51.3-deg slope" and "60-deg incident angle" represents these rays, which comprise more than half the wave front at ray angles above 25 degrees. The reflected energy from these rays will be directed backward to the backscattered region.

The direction that a reflected ray leaves the keel, θ_r, is given by $\theta + 2\phi$. Figure 13 shows these reflected angles for an incident wave front of 20 degrees. The line labeled "slope angle" is the slope on the keel and is equivalent to the angles along the 20-degree abscissa in Fig. 12. The reflected angle is then twice this slope plus 20 degrees for the direct rays on the right side of the figure. At a wave front location of -2.2 m, the rays become surface-reflected, and θ is

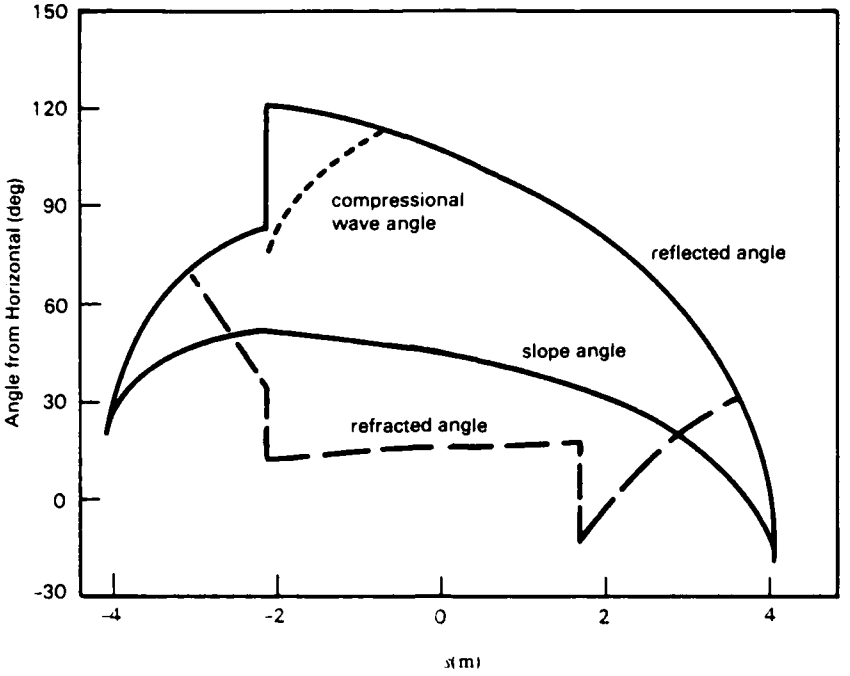

Figure 13. Angles at which rays emerge after striking or passing through the keel of Fig. 10, as a function of position on the wave front. The slope of the keel at the point of contact is labeled "slope angle."

-20 degrees. This causes the vertical discontinuity of 40 degrees in the reflected angle. Reflected angles less than 0 degrees are headed upward after reflection and reflect from the surface behind the keel, becoming downgoing or positive angles of the same size.

The final angle at which refracted rays emerge from the keel cannot be easily characterized. Figure 14 shows the change in angle at the interface for the water wave to ice shear wave interaction for the sound speeds of Table 1. A 45-degree line is drawn in to indicate the size of the angle change. At high grazing angles or near-normal incidence, very little change occurs. These angular changes occur at transmission both into the keel and from it. The additional change in ray angle is a result of change in slope of the keel at the entering and exiting points. The ray may also reflect from the flat upper surface of the keel model.

A compressional wave begins when the grazing angle equals 66 degrees and ends when the rays reach the upper corner of the keel. The upper end of this line has a small transmission coefficient, but towards the lower end provides occasional downward-directed rays, as can be seen in Fig. 4 and other such scatter diagrams.

The accumulation of the above effects produces exiting angles for a 20-degree ray set, shown by the dashed lines in Fig. 13. At the critical grazing angle near 26 degrees, the reflected and refracted rays correspond in angle. The dashed line therefore meets the reflected angle curve at the points where the slope angle is 26 $\pm$ 20 degrees. The nearly flat section through the middle of the refracted angle line is from rays that reflect from the upper surface of the keel. The discontinuity at either end of this section is the ray that intersects either the leading or trailing corner of the keel and surface.

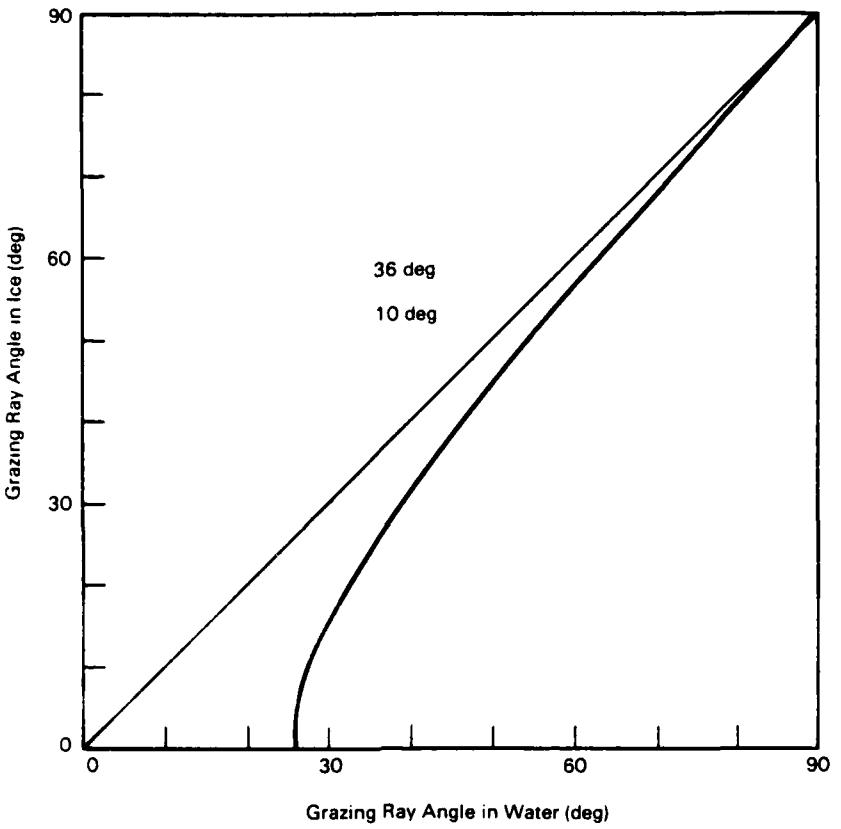

Figure 14. Refraction angle at water-ice interface for the water wave and ice shear wave.

The final scattering function for a single keel is the convolution of the angles of Fig. 13 with the reflection losses of Fig. 5. However, the transmission losses of Fig. 5 contain ray-spreading terms that must be removed, since equal intervals along the *s* scale of Fig. 12 represent equal energy, and spreading effects are built in.

MODEL SHORTCOMINGS

The models used here fail to represent reality in many ways. Some of their shortcomings are listed here. The results of limitations on slope angles were discussed in the section on backscatter. Perhaps the next most noticeable shortcoming is the absence of reflection from the far sides of the keels. These reflections might add significantly to the backscattering strengths of the keels. In a pure ray construction treatment, as used here, one must terminate internal reflections at some number or level. Here, they were terminated at zero.

A third important shortcoming is the absence of an ice plate which could alter ray paths. This shortcoming does not cause serious angular dislocations though, because the transmission coefficient is such that rays directed into the ice plate will readily pass back into the water. A nonflat upper ice surface, however, will disturb ray paths.

Finally, attenuation of shear waves in the ice is omitted. This may very well add a decibel or more loss to paths through the ice, changing the angular scattering diagram. This effect and others upon the reflection coefficient at the ice plate might reduce the specular reflection coefficient, which depends upon reflection from the plate.

CONCLUSIONS

A collection of ice keels has been modeled by parabolas that have distributions of size and spacing that match estimates of real keels. Rays representing a plane wave have been scattered from this set of keels, with resultant scattering angles and specular reflection coefficients.

The reflection-transmission characteristics of the water-ice interface are shown to be important in determining the angles into which energy is scattered. The particular geometric properties of the parabolas also have a strong effect on the estimated scattering angles. This is particularly true of backscatter, which is underestimated by the parabolic shapes.

Specular reflection coefficients from the keels are estimated by computing the ratio of shadowed surface to total surface.

For grazing angles up to 20 degrees, transmission through the keels accounts for more scattered energy than reflection from the keel. Below 20 degrees, this transmission is predominantly by shear waves rather than compressional waves.

RECOMMENDATIONS

The ray theory program utilized here permits keel shapes to be approximated by several parabolic or straight-line segments, although only a single parabolic segment per keel was used here. Such compound shapes could more nearly model real keels. Because the shapes used here lead to defective estimates of backscatter, the use of compound shapes is particularly indicated for keel backscatter estimations.

Before more appropriate keel shapes are generated, much information is needed about detailed keel shape and structure. If keels tend to remain collections of independent ice blocks or slabs throughout their life, then the current analysis, which is based on solid ice shapes, has very limited validity. If keels do solidify and if their shape is modified by local melting and freezing, then a solid ice model can be appropriate. Clearly, a great deal of observed information on shapes and slopes is needed to produce random model shapes that match readily. Upsounder echo traces might serve as sources of this needed information.

If acoustic paths through ice keels are important, as the current analysis indicates, then the internal elastic-acoustic properties and degree of homogeneity of keels is important. Of particular importance are the sound speed and the attenuation of the two wave types, shear and compressional. A systematic study of the ice in keels is needed.

Acoustic experiments performed in the vicinity of a well-observed keel could reveal much about the acoustic properties of keels. The basic requirements are receivers at several depths, both in front of and behind the keel, and a variable source angle. The ability to separate multipath arrivals would also be useful.

REFERENCES

1. D.F. Gordon, *Ray Theory Computer Program for Determining Acoustic Effects of Ice Keels*, NOSC TR 1099, Apr 1986.
2. O.I. Diachok, "Effects of Sea-Ice Ridges on Sound Propagation in the Arctic Ocean," J. Acoust. Soc. Am., **59**, pp 1110–1120, May 1976.
3. Chin-Bing, S.A., "The Influence of Water-to-Ice Transition Layers on the Reflection Coefficient and High-Frequency Acoustic Backscatter from an Ice Keel," J. Acoust. Soc. Am., Suppl. 1, **78**, S57, 1985.
4. W.M. Ewing, W.S. Jardetsky, and F. Press, *Elastic Waves in Layered Media*, McGraw-Hill, NY, 1957.
5. W.G. Mayer, M. Behravesh, and T.J. Plona, "Determination of Sonic Velocities from Reflectivity Losses at Sea Ice Boundaries," J. Acoust. Soc. Am., **57**, pp 39–46, Jan 1975.

END
DATED
FILM
8-88
DTIC